Essential Readings in Light Metals: Electrode Technology for Aluminum Production.
Edited by Alan Tomsett and John Johnson.
© 2013 The Minerals, Metals & Materials Society. Published 2013 by John Wiley & Sons, Inc.
Light Metals — From ***Light Metals 1989***, Paul G. Campbell, Editor

A COMPREHENSIVE DETERMINATION OF EFFECTS OF CALCINED PETROLEUM COKE PROPERTIES ON ALUMINUM REDUCTION CELL ANODE PROPERTIES

David Belitskus and Daniel J. Danka
Aluminum Company of America
Alcoa Laboratories
Alcoa Center, PA 15069, U.S.A.

ABSTRACT

A bench scale determination of effects of calcined coke properties on prebaked anode properties was made using 16 cokes. Coke physical and chemical analyses included bulk and real densities, crystallite height, electrical resistivity, BET surface area, mercury porosimetry, and impurity analyses. Anode density, electrical resistivity, excess electrolytic consumption, and air burning rate were determined. Least squares regression analyses were carried out. Anode density correlated well with coke vibrated bulk density and coke porosity below 5 μm in diameter. Electrical resistivity correlated very well with coke resistivity, along with vibrated bulk density. Air burning to a 10% weight loss correlated only with mercury porosimetry values, although rate toward the end of the experiments increased with coke vanadium content. Consumption during electrolysis correlations were weak, but consumption increased with metallic impurities such as nickel.

INTRODUCTION

Calcined petroleum cokes used in aluminum reduction cells can vary appreciably in both physical properties and chemical impurity levels. Although it is known that such differences can contribute to variations in anode performance, published works on the subject are, for the most part, limited in scope and sometimes contradictory. Some examples of published findings are given below.

Rhedey (1) reported that anode air burning increased with increasing vanadium, nickel, and calcium levels, but was not affected by sulfur, iron, silicon, or total ash contents. In more recent work, Houston and Øye (2) and Schmidt-Hatting et al. (3) indicated a detrimental effect of vanadium on anode consumption, and Rhedey and Nadkarni (4) reported that both vanadium and nickel increased air burning and that high coke porosity had a negative effect on anode properties. Keller and Fischer (5) claimed that sodium increases anode consumption, but gave no supporting data. A detrimental effect of sodium on anode reactivity with carbon dioxide was also reported in Reference 2.

In other work, Rhedey (6) found that excess electrolytic anode consumption decreased with increasing coke vibrated bulk density, decreasing calcination temperature, and increasing sulfur content. In contrast to one of these findings, Kolodin and Nikitin (7) reported decreased excess electrolytic consumption with increasing coke real density (which increases with calcination temperature). The same workers reported increased consumption with increasing coke ash content.

In contrast to another finding in Reference 6, Jones et al. (8) showed an increase in anode consumption in commercial cells with increasing coke sulfur content. Burnakin et al. (9) also reported increasing anode consumption with increasing coke sulfur content. Barrillon and Pinoir (10) reported that anode consumption increases as more sulfur is lost during anode baking, but presented no data. In a review article, Houston and Øye (11) gave a more complete summary of published findings on coke impurity effects on carbon air burning and reactivity with carbon dioxide.

Jones and Hildebrandt (12) reported that anode consumption increases as coke porosity in the 1-10 μm diameter range increases. Nikitin et al. (13) found that anode baked apparent density increased and electrical resistivity decreased as coke real density increased. Gehlbach et al. (14) showed that an increase in anode baked apparent density correlated well with an increase in -20+48 mesh coke vibrated bulk density, but not as well with other coke bulk density measurements or with mercury porosimetry values. These workers also found an inverse correlation between -20+48 mesh coke vibrated bulk density and optimum anode binder content.

Holdner and DuTremblay (15) claimed a good correlation between the vibrated bulk density of a sized coke aggregate and optimum anode binder content. Tonti et al. (16) proposed a relationship between anode baked apparent density and coke vibrated bulk density and isotropy, where coke pore volume down to 5 μm in diameter was used as an indicator of coke isotropy.

Probably the most comprehensive study of the effects of coke properties on anode properties was carried out by Lazarev et al. (17), who measured eight coke properties and five anode properties with twenty coke samples, However, no multivariable data analyses were performed and none of the correlations between a single coke property and an anode property had a particularly high degree of statistical significance.

The work described in the present publication was carried out to broaden the range of coke and anode properties measured, to provide statistically valid correlations among properties, and to explain these correlations in terms of chemical and physical interactions.

COKE SAMPLE ORIGINS

Most of the cokes used in this study were commercially available calcined cokes that have been used in aluminum reduction cell anodes. Use of commercially calcined coke was disadvantageous from the standpoint of superimposing effects due to coke calcining variables and effects due to green coke variables, but the advantage of studying cokes as they are received by commercial aluminum reduction operations was felt to outweigh this disadvantage.

Two of the samples were not commercially calcined cokes. One coke (No. 4) was partially desulfurized in a vertical shaft pilot calciner using a higher than normal maximum temperature and an unspecified chemical reducing treatment. Another coke (No. 6) was calcined in the laboratory at a slow up-heat rate, giving a lower than typical porosity. About half of the samples were crushed in commercial anode plants; the remainder were crushed in the laboratory.

COKE PROPERTIES

The coke properties determined are described below and values are given in Appendix I. Because the number of coke properties determined is quite large, 152, only the range in each property is reported herein (Appendix I). The complete data will be supplied by the authors on request.

Vibrated Bulk Density

Vibrated bulk densities of coke fractions ranging from -4+8 mesh to -200 mesh were determined using Alcoa Method 424C (which is the same as ASTM Test Method D4292 for fractions down to -28+48 mesh). Values are shown in Figure 1. For many of the cokes, vibrated bulk density of a sized aggregate (10 wt% -4+8 mesh, 19 wt% -8+14 mesh, 14 wt% -14+28 mesh, 12 wt% -28+48 mesh, 10 wt% -48+100 mesh, 14 wt% -100+200 mesh, 21 wt% -200 mesh) was determined also.

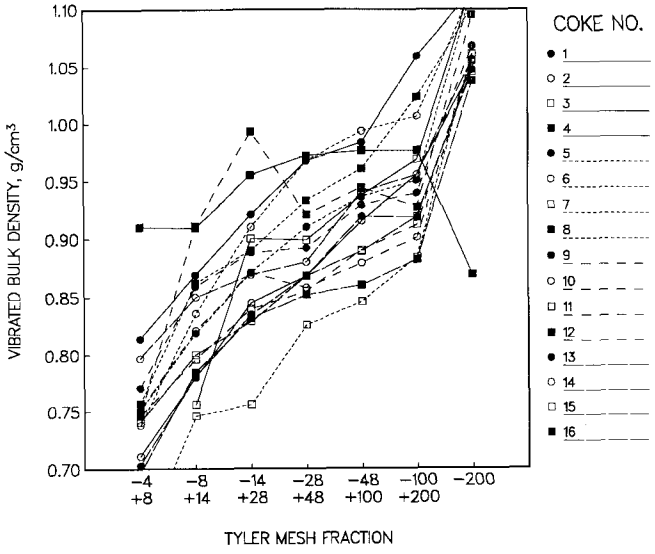

Figure 1. Vibrated bulk densities of calcined coke samples as a function of particle size.

Real Density

Real densities were determined for each coke by two methods, kerosine displacement and helium displacement. Alcoa Method 424F was used for the kerosine displacement determinations. The helium displacement determinations utilized a Micromeritics Autopycnometer Model 1320.

Crystallite Height (L_c) and Estimated Calcination Temperature

Crystallite height determinations were made using a Siemens Model D500 X-ray diffractometer.

Coke calcination temperatures were estimated by heating samples of each coke at temperatures ranging from about 1000 to 1400°C and redetermining L_c after each heat treatment. The temperature at which a coke was originally calcined was estimated to be the highest temperature prior to a significant increase in L_c. The curves used for these estimates are shown in Figure 2.

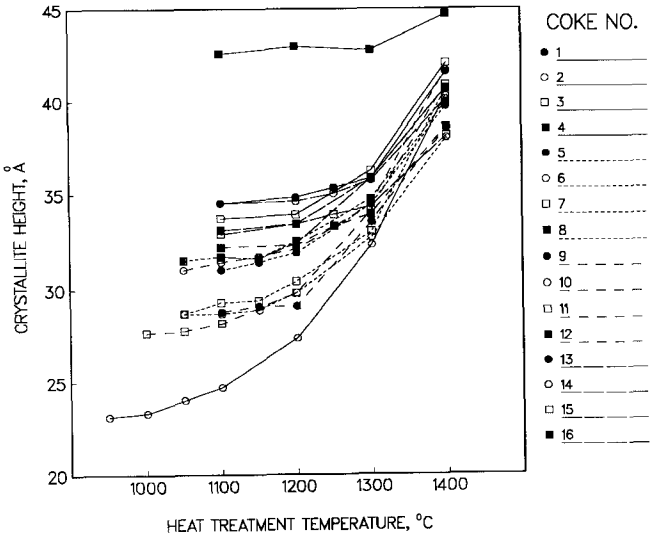

Figure 2. Crystallite height values for calcined coke samples after various heat tretment temperatures.

Electrical Resistivity

Particle electrical resistivities were measured on -28+48, -100+200, and -200 mesh fractions using apparatus built by Airco Carbide for determining calcined anthracite resistivities. A pressure of 4.1 MPa (600 psi) was applied.

Characterization of -200 Mesh Particle Size Distribution

Characterization of the particle size distribution in the -200 mesh fraction was carried out using an L&N Microtrac particle size analyzer. Reported values include particle diameters below which 10, 50, and 90 wt% of the particles are found, and the average particle diameter. Although fineness of the -200 mesh fraction is not an intrinsic coke property, it was measured so that possible effects on anode properties could be assessed.

Mercury Porosimetry

Mercury porosimetry measurements were made using a Micromeritics Auto Pore 9200 (0-60,000 psi) on four coke fractions: -4+8, -28+48, -100+200, and -200 mesh. This instrument yields a number of values,

including total intrusion volume, total pore area, three types of calculated pore diameter, and two types of calculated density.

In addition, fractions of the total porosity in various pore size ranges are given. Using these data, many additional types of values were calculated. Descriptions of both the values given directly and the additional calculated values are given in Appendix II.

Surface Area

Surface areas were measured by the BET method using a Micromeritics Digisorb 2600 with krypton gas for four coke fractions: -4+8, -28+48, -100+200, and -200 mesh.

Chemical Analyses

Elemental analyses were obtained for aluminum, calcium, fluorine, iron, nickel, potassium, silicon, sodium, sulfur, and vanadium, and total ash was determined. Most of the chemical analyses were done by atomic absorption or atomic emission, using standard Alcoa techniques. Fluoride was determined using a standard wet method. Sulfur was determined using a Leco Model SC-132 sulfur analyzer.

ANODE FABRICATION

Bench scale anodes were fabricated from each of the cokes, using a constant sizing by weight. The particle size distribution selected was given earlier in the section on vibrated bulk density determinations. Several binder pitch levels were used so that each coke could be tested with its optimum binder level and so that optimum level as a function of coke properties could be investigated. Binder was a coal tar pitch having a 113°C softening point (Mettler method), a quinoline insoluble content of 11.5 wt%, an aromaticity of 96% by nuclear magnetic resonance, and a Conradson coking value of 59%.

One-kilogram mixes were blended at 140°C for 30 minutes in a 3.8 litre (1-gal) sigma-blade mixer. Fifty-millimeter diameter, approximately 125 mm long specimens were formed at 140°C under a pressure of 27.6 MPa (4000 psi).

Anodes were baked in a resistance heated furnace in packing coke and under a nitrogen flow. Up-heat rate was 25°C/h to a maximum temperature of 1125°C and soak time was ten hours.

MEASUREMENT OF ANODE PROPERTIES

Green and baked apparent densities were calculated from weights and volumes before and after baking, with volumes determined by water displacement. Calculated aggregate densities in green anodes were determined from the relationship: calculated bulk density = green apparent density x (100-%pitch)/100.

Electrical resistivities at room temperature were determined using the four-point method. Resistivity was calculated from the voltage drop along a 25 mm anode section passing 6A of current.

Green and baked apparent densities, volume changes during baking, and electrical resistivities are shown in Figures 3-6. Optimum anode binder pitch levels were estimated from the baked apparent density and electrical resistivity data. In several cases, optimum level was not clear cut.

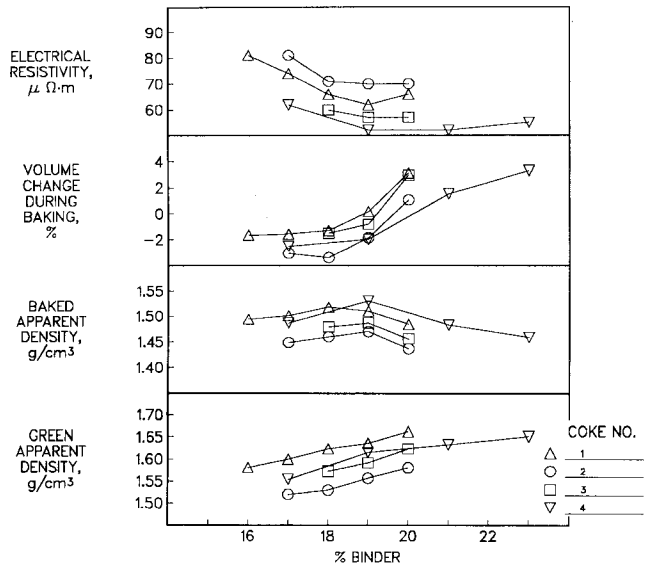

Figure 3. Anode properties as a function of binder level for Cokes 1 to 4.

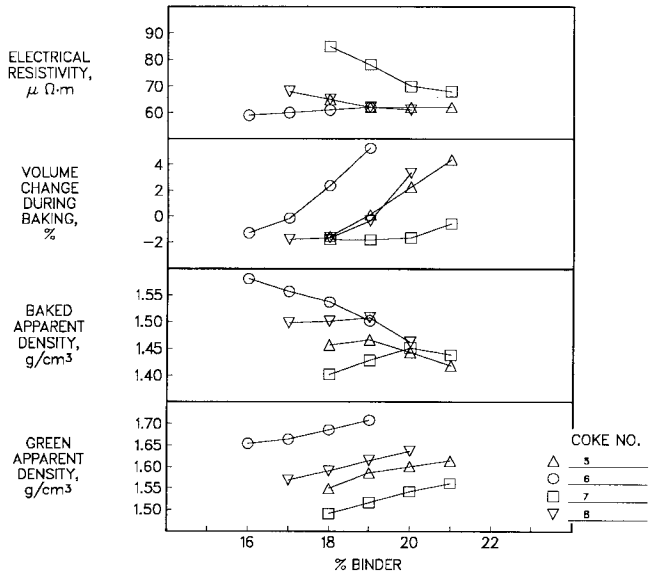

Figure 4. Anode properties as a function of binder level for Cokes 5 to 8.

Excess anode consumption during electrolysis and air oxidation rates were determined only for anodes having optimum binder levels. In the cases where optimum level was not easy to estimate, two sets of samples with pitch levels around the optimum were used in the electrolytic consumption test. Consumption values for the two sets were similar in all cases.

Consumption during electrolysis was determined using an Alcoa-design bench scale cell. Conditions were: a bath ratio of 1.20, a temperature of 980°C, 6 wt% calcium fluoride in the bath, 5 wt% alumina in the bath, and a current density of 1.1 A/cm^2. Four to eight replicate determinations were generally made for each type of anode. Results for some of the anodes had high standard deviations (Table II).

Table I. Optimum Binder Level and Properties of Anodes Produced with the Optimum Level

Arbitrary Coke Number	Optimum Binder Level, wt%	Apparent Density, g/cm³		Electrical Resistivity, μΩ•m	Air Burning Rate, mg/h/cm²		Consumption During Electrolysis, % of Theoretical
		Green	Baked		Average	Final	
1	19	1.643	1.521	64	61.0	360	107.2 *
2	19	1.557	1.470	70	58.0	421	107.4
3	19	1.592	1.487	57	79.5	445	106.6
4	19	1.616	1.531	52	78.5	505	105.5
5	18	1.584	1.480	62	60.5	360	107.0
6	16	1.653	1.581	59	83.0	398	107.3 *
7	21	1.561	1.438	68	28.5	126	106.4 *
8	19	1.615	1.508	60	33.0	189	105.0
9	18	1.603	1.517	62	89.0	541	106.1
10	18	1.560	1.469	61	46.0	280	105.6 *
11	19	1.583	1.500	66	72.0	473	105.6 *
12	17	1.582	1.510	57	96.0	398	108.2 *
13	19	1.549	1.455	65	41.5	344	107.2
14	19	1.588	1.474	61	47.5	421	106.2
15	19	1.584	1.469	65	37.0	222	106.6
16	19	1.545	1.453	65	44.0	344	106.7

* Average of 2 binder levels.

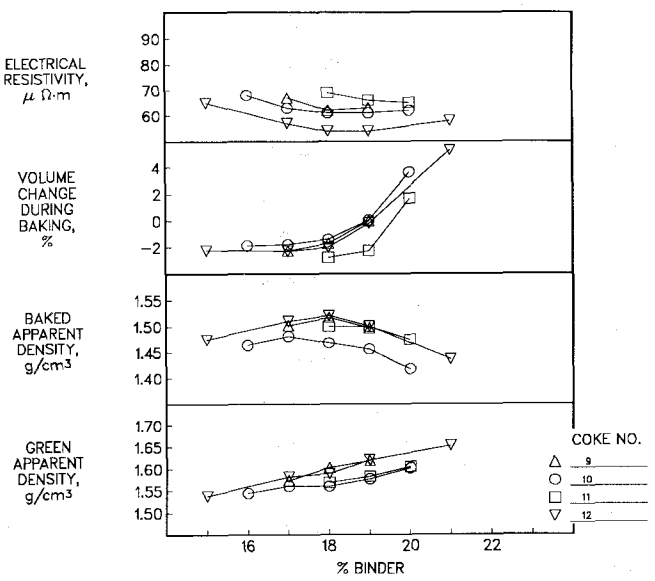

Figure 5. Anode properties as a function of binder level for Cokes 9 to 12

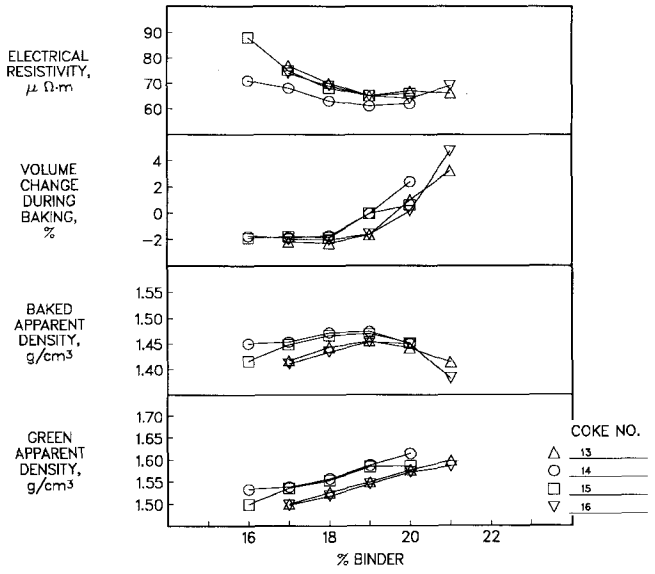

Figure 6. Anode properties as a function of binder level for Cokes 13 to 16.

Air burning rates were measured at 550°C in a flowing stream of air, using a continuously recording microbalance.* The ends of each cylindrical 25 mm long, 12.5 mm diameter test specimen were fitted with ceramic covers so that oxidation was essentially restricted to the vertical surface. Runs were carried out to a 10% weight loss and rate was expressed in terms of geometric surface area. A second rate was calculated based only on the last 30 mg of weight loss in an attempt to distinguish between factors that contributed to the onset of rapid air burning and those that affected the more rapid, essentially linear rate later in the run. Duplicate tests were run in all cases. Overall weight loss curves are shown in Figure 7.

*These measurements were made at the U.S. Steel Corporation chemicals laboratory (now the Aristech Chemical Corporation Laboratory) in Monroeville, PA.

Table I gives values for optimum binder levels and properties of anodes produced with the optimum levels.

CORRELATION STRATEGY

Data analysis was carried out using the ALSTAT program (19) on a DEC10 computer. The primary method of analysis was multivariable linear ridge regression. In some cases, least squares cubic spline (curvilinear) regressions were investigated also, but in general these were not significantly better than the linear regressions.

Since the number of coke properties measured and calculated far exceeded the number of cokes tested, multiple regression analyses including all the coke data were not possible. Instead, most analyses consisted of trials of each coke property with each anode property and of all combinations of two coke properties with each anode property.

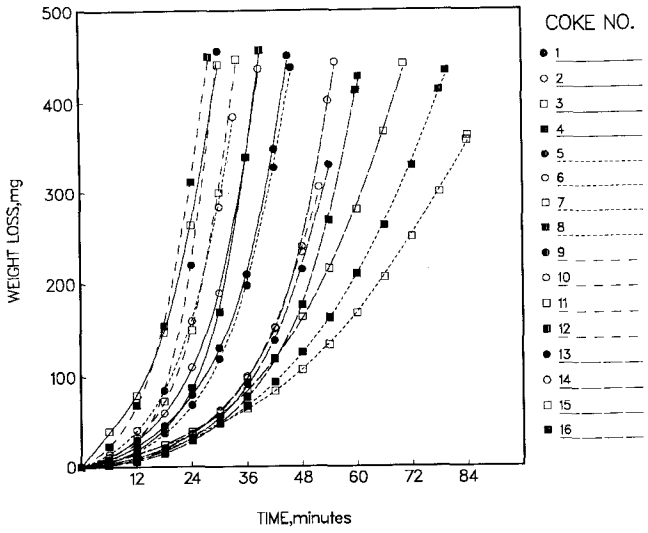

Figure 7. Weight losses of anode samples oxidized in air at 550°C as a function of time.

Selected regression equations including more than two independent variables were tested also, but in the final analysis, use of a third variable was not considered justifiable for any of the anode properties.

Although there are a number of ways of expressing the effectiveness of a regression equation in correlating the dependent variable with the independent variables, the multiple correlation coefficient squared x 100, or "R^2", is commonly reported and will be used in this publication.

A few words should be given on the significance of results of regression analyses. Younger (20) considers a correlation coefficient of 0.75 (R^2=56%) to represent a moderately strong correlation and 0.50 (R^2=25%) to represent a moderate correlation. In this work, most of the R^2 values for the regression equations considered to be most appropriate are >75%.

It should be mentioned also that a multiple regression model is greatly dependent upon the criteria applied in selecting the variables to be tested (21). When there are a large number of independent variables and no one or two of them overwhelmingly dominate the value of the dependent variable, a number of models can yield nearly equivalent R^2 values. This is especially true when many of the independent values are correlated with each other. Thus, the models given in this report seem reasonable in terms of relatively high R^2 values and in terms of the particular coke properties used in the models, but are somewhat subjective.

CORRELATIONS AMONG COKE PROPERTIES

Prior to investigating coke properties versus anode properties, correlations among various coke properties were sought. Results are summarized below.

All values from Microtrac particle size analysis of the -200 mesh fraction correlated well with each other, with R^2 values ranging from 58 to 98% for the six combinations of the four reported types of values. Hence, a single number such as the average particle diameter adequately describes the fineness of this fraction.

Table II. Summary of Excess Electrolytic Consumption Values

Coke Number	Number of Test Specimens Run	Average Value, % of Theoretical	Standard Deviation % of Theoretical
8	4	105.0	0.2
15	4	106.6	0.2
13	4	107.2	0.4
1	12	107.2	0.4
14	4	106.2	0.5
7	8	106.4	0.5
5	4	107.0	0.5
2	8	107.4	0.6
12	7	108.2	0.6
10	8	105.6	0.7
9	8	106.1	0.7
11	8	105.6	0.9
6	8	107.3	0.9
16	4	106.7	0.9
3	3	106.6	1.2
4 *	8	105.5	1.4

*Not included in regression analyses

Coke properties that were measured on several fractions were examined with respect to differences among fractions. BET surface area correlated to some extent among fractions. (For the six combinations of the four fractions used, R^2 values ranged from 19 to 82%.) Surface areas for the four fractions probably correlate to some extent because fine pores tend to dominate this measurement.

In contrast, the mercury porosimeter values did not correlate at all among fractions, except for total pore area. The ranges in R^2 values for total pore area corresonding to the six combinations of the four fractions used were 30-93%. Most R^2 values for the other types of reported mercury porosimeter values were well below 50%.

Apparently, total pore area correlates to some extent for different size particles of a given coke for the same reason that BET surface area does, i.e., this value is dominated by the fine pore structure.

This work reaffirms an earlier conclusion (18) that vibrated bulk densities of calcined coke sized fractions correlate to some extent with other fractions, except for the -200 mesh fraction. Most values of R^2 from two-variable correlations between fractions (excluding -200 mesh) ranged from 43-89%.

In general, BET surface areas for a coke fraction did not correlate with vibrated bulk densities for the same fraction, although there was a moderate correlation with -28+48 mesh coke (R^2=48%). Since the surface area measurement is affected by pore size and vibrated bulk density is an indicator of total porosity, the lack of correlation between these types of measurement is not surprising.

Very few of the mercury porosimetry values correlated with vibrated bulk density. R^2 values for two-variable correlations for comparable size fractions were generally below 50%.

Concerning coke variables expected to be affected by calcination, real density by kerosine displacement and by helium displacement correlated quite well

(R^2=76%, or 85% when one outlier is excluded). Neither real density correlated particularly well with crystallite height (R^2=40% for real density by helium, 34% for real density by kerosine). Estimated calcination temperature correlated well with crystallite height (R^2=82%), but not as well with real density (R^2=59% for helium, 45% for kerosine).

The better correlation with crystallite height agrees with the conclusion of Rhedey (22). Probable reasons are that crystallite height increases by a greater percentage than real density over the maximum temperature range of commercial calcination and that real density of high sulfur coke can decrease slightly with increasing temperature as sulfur-containing species are volatilized.

The regression equation for estimating calcination temperature from crystallite height is:

Estimated calcination temperature (in °C)
= 640 + 17.2 L_c (in Å)

ANODE PROPERTIES VS. COKE PROPERTIES

Green Apparent Density

The type of coke property measurement that gave the best correlation with anode green apparent density at the optimum binder level is vibrated bulk density. The best correlation was with the sum of the -28+48, -48+100, and -100+200 mesh densities (R^2=76%). However, the -28+48 mesh density alone gave a correlation nearly as good (R^2=73%). The next six best correlations (R^2=65-70%) also involved various vibrated bulk density values.

When two coke properties were correlated with green apparent density, the five best equations (R^2=88-93%) involved an average vibrated bulk density value and a mercury porosimetry value (or a displacement density, which combines mercury porosimetry and real density values). Two of the nine best two-coke-property correlations involved -28+48 mesh coke vibrated bulk density and four involved -28+48 mesh coke displacement density including pores below 5 µm in diameter. Although an equation combining these two coke measurements did not result in the highest R^2 value (87%), it is considered the most reasonable equation since it involves a single coke fraction for both of the measurements. Inclusion of a displacement density term supports published work (16).

When three coke variables were tried in correlations with green apparent density, well over one hundred regression equations had R^2 values over 90%. Most of the better equations included a vibrated bulk density term and two mercury porosimetry terms. Since no different kinds of coke properties generally appeared as the third term, reporting of a correlation using three coke variables is not considered justifiable. Hence, the most suitable regression equation for green apparent density is judged to be:

Green apparent density (in g/cm^3)
= 0.60 + 0.56 x vibrated bulk density of -28+48 mesh coke (in g/cm^3)
+ 0.28 x 5 µm displacement density of -28+48 mesh coke (in g/cm^3)

Relative influences:		
	vibrated bulk density	62%
	displacement density	38%

Observed vs. predicted values from this equation are shown in Figure 8.

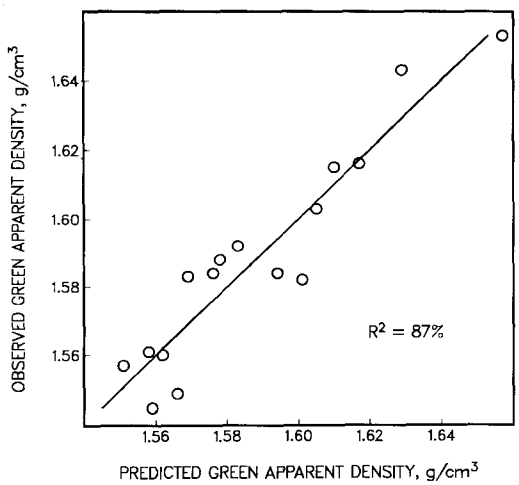

Figure 8. Comparison of observed and predicted anode green densities.

It seems reasonable that an equation including a coke vibrated bulk density term and a term indicating coke "microporosity" predicts anode green apparent density well. Vibrated bulk density gives an indication of overall coke porosity, but under the experimental conditions used, pores below about 5 µm in diameter were probably not penetrated by pitch. Hence, for a given coke vibrated bulk density, green apparent density increases as the fraction of the total porosity above 5 µm in diameter increases. Measurements on -28+48 mesh coke are probably superior to measurements on other fractions because this fraction is about midrange of the fractions used in anode manufacture and gives close to an average value for vibrated bulk density and displacement density.

Baked Apparent Density

Vibrated bulk density of the -28+48 mesh coke fraction was the best single coke variable correlating with anode baked apparent density (R^2=70%). Other vibrated bulk density values resulted in the next five best regression equations (R^2=61-67%).

When two coke variables were used, the same variables judged to most reasonably predict green apparent density predicted baked apparent density with an R^2 value of 82%. The best equation, however, was slightly different, utilizing -28+48 mesh coke vibrated bulk density and -28+48 mesh coke pore volume below 5 µm in diameter (R^2=90%). Although the specific term relating to coke "microporosity" differs in the equations for green apparent density and baked apparent density, this difference is probably of no great significance since so many equations combining coke vibrated bulk density and mercury porosimetry data involving porosity below about 5 µm in diameter predict green and baked apparent densities quite well.

The use of a third coke variable in regression equations predicting baked apparent density raised R^2 to as high as 96%. However, since most of the better equations included only combinations of vibrated bulk density and mercury porosimetry terms, inclusion of a third term does not seem warranted. Hence, the equation deemed to be most reasonable for predicting anode baked apparent density is:

Baked apparent density (in g/cm^3)
= 0.98 + 0.68 x vibrated bulk density of -28+48 mesh coke (in g/cm^3)

- 1.21 x microporosity <5 μm in diameter in -28+48 mesh coke (in cm^3/g)

Relative influences:	vibrated bulk density	61%
	microporosity	39%

Observed and predicted values are shown in Figure 9.

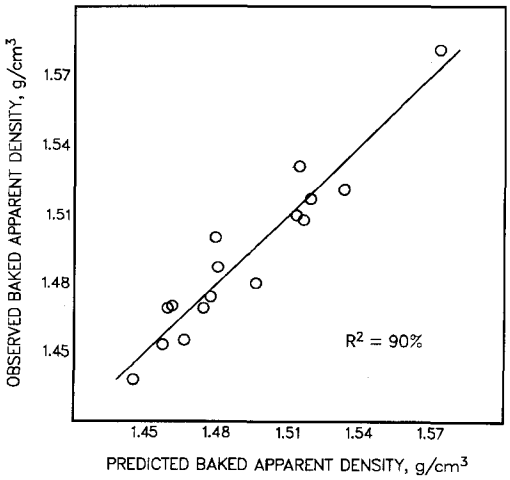

Figure 9. Comparison of observed and predicted anode baked apparent densities.

Optimum Binder Level

Optimum binder levels could not be estimated from the experimental data to any closer than whole percentages and, in some cases, even these estimates were doubtful (Figures 3-6).

In regression equations involving only one coke variable, four values derived from mercury porosimetry predicted optimum pitch level best (R^2=39-46%). The -14+28 mesh vibrated bulk density was next best, with an R^2 of 37%.

Many of the correlations involving two coke variables included -14+28 mesh vibrated bulk density and mercury porosimetry terms. The best regression equation (R^2=66%) included -14+28 mesh coke vibrated bulk density and -28+48 mesh coke volume of pores below 5 μm in diameter.

Although aggregate bulk density has been reported to correlate well with optimum binder level (15), correlation was not very good in this work (R^2=35%). It can be noted that when the "aggregate density" in a green anode was calculated according to the equation given previously, correlation with measured aggregate vibrated bulk density was only moderately strong (R^2=65%). This is another indication that pore size distribution (especially, the fraction of the porosity below about 5 μm in diameter, which is not accessible to pitch) is important.

The selected regression equation is:

Optimum binder pitch level (in wt%)
= 26.2 - 13.2 x vibrated bulk density of -14+28 mesh coke (in g/cm^3)

+45.5 x microporosity <5 μm in diameter in -28+48 mesh coke (in cm^3/g).

Relative influences:	vibrated bulk density	57%
	microporosity	43%

Figure 10 shows that this equation adequately predicted which cokes required a high or low pitch level but did not differentiate well among most of the cokes. This may be due in large part to the uncertainty in the optimum pitch levels estimated from the experimental data.

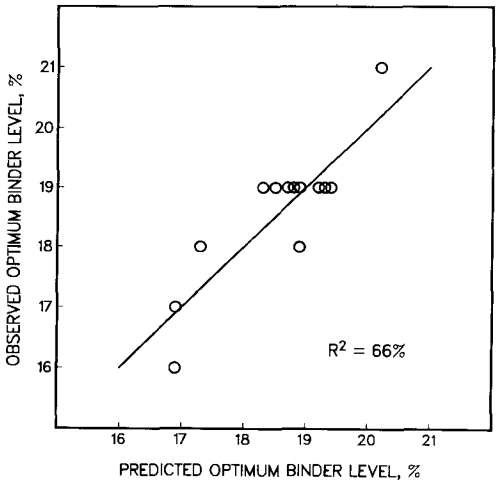

Figure 10. Comparison of observed and predicted optimum anode binder levels.

Electrical Resistivity

The best correlation of an anode property with a single coke property was anode electrical resistivity with electrical resistivity of the -100+200 mesh coke fraction (R^2=91%, excluding one significant outlier*). Equations using resistivity values of other coke fractions were not nearly as good (R^2=74% for -48+100 mesh coke, 59% for -200 mesh coke).

The ten best two-coke-variable correlations included -100+200 mesh coke particle resistivity and either a vibrated bulk density or a mercury porosimetry term (R^2=95-98%). Since the least complicated coke measurements were judged to be the most useful, the best correlation using vibrated bulk density of a single fraction, as opposed to an average, is given below (R^2=96%).

Anode electrical resistivity (in μΩ• m)
= 58.7 + 0.054 x electrical resistivity of -100+200 mesh coke (in μΩ•m)

-26.6 x vibrated bulk density of -48+100 mesh coke (in g/cm^3).

*For an undetermined reason, the value for coke No. 10 appreciably degraded all the resistivity correlations, so it was excluded from the analyses.

Relative influences: electrical resistivity 80%
vibrated bulk density 20%

Figure 11 shows observed vs. predicted values.

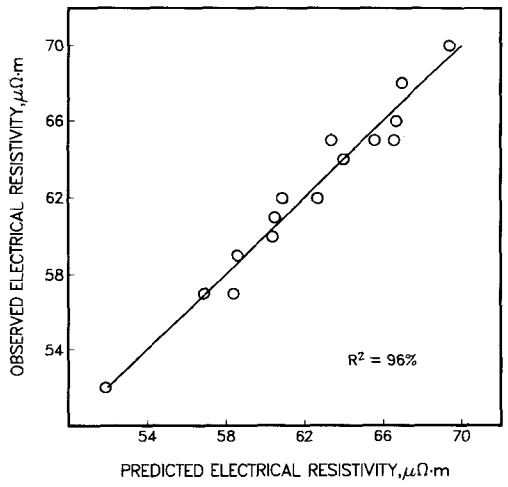

Figure 11. Comparison of observed and predicted anode electrical resistivities.

The fact that both the electrical resistivity and vibrated bulk density values in the best equation involved relatively fine particle sizes indicates that the finer particles in an anode carry a significant fraction of the total current.

Air Burning

The ten best equations (R^2=53-72%) correlating average anode air burning rate to a 10% weight loss with one coke property involved -4+8 mesh coke mercury porosimetry values. The best correlation was with total mercury intrusion volume. Most of the best two-coke-variable correlations included this coke property and a -200 mesh coke mercury porosimetry value. The best correlation (R^2=83%) was with incremental volume at 23 μm pore diameter, but correlation was only slightly poorer (R^2=82%) with one of the basic mercury porosimetry values, skeletal density, so this equation is deemed to be most suitable:

Average air burning rate (in mg/h/cm^2)
= 224 - 531 x total intrusion volume of -4+8 mesh coke (in cm^3/g)

-34 x skeletal density of -200 mesh coke (in g/cm^3)

Relative influences: intrusion volume 76%
skeletal density 24%

Observed vs. predicted values are shown in Figure 12.

Although it is not surprising that anode air burning rate would correlate with porosity factors, the reasons for the particular factors involved and the direction of the total intrusion volume effect are not obvious. As total intrusion volume increased, air burning rate decreased. Intuitively, the opposite effect might be expected. However, it may be noted that only anodes having the optimum binder level were tested for air burning rate and that there is a moderately good direct correlation (R^2=48%) between

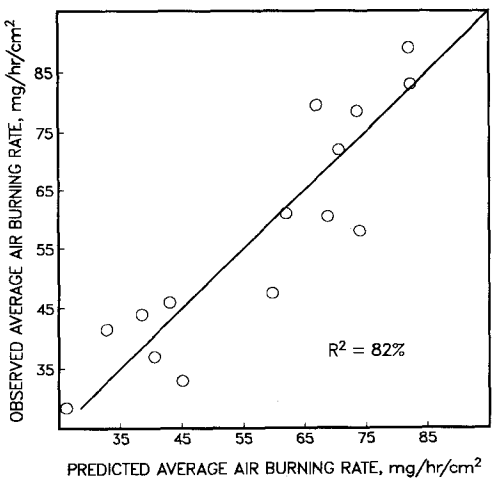

Figure 12. Comparison of observed and predicted anode air burning rates to 10% weight loss.

-4+8 mesh coke total mercury intrusion volume and optimum anode binder level. Hence, the best anodes from an air burning standpoint tended to have the highest pitch levels. It is possible that much of the surface accessible anode porosity in the machined air burning test specimens is due to the exposed interiors of coarse coke particles not penetrated by coked pitch. When the interiors of the coarse particles are penetrated by coked pitch to a greater extent, less porosity may be exposed.

An increase in coke skeletal density implies an increase in the graphite-like character of the carbon and/or a decrease in the microporosity, both of which would be expected to decrease air burning rate. Possibly, the -200 mesh coke skeletal density gave a good correlation because this fraction has the largest geometric surface area for a given weight and, therefore, is the most accessible to oxygen.

Although coke vanadium content has been reported to correlate very well with anode air burning rate (1), there was little statistical basis in this work for attributing an increase in average anode air burning rate to a 10% weight loss to an increase in coke vanadium content (R^2=27%). Figure 13 is a plot of average anode air burning rate vs. coke vanadium content. However, when only the rate toward the end of the air burning test (last 30 mg, or approximately the last 1%, of weight loss) was considered, coke vanadium content resulted in the fourth best single-coke-variable correlation (R^2=55%), behind three -4+8 mesh coke mercury porosimetry values (highest R^2=60%). The R^2 value increased to 71% for coke vanadium content when a curvilinear equation was used. Figure 14 shows rate during the last 30 mg of weight loss vs. coke vanadium content.

It is probable, then, that coke porosity factors exert the major effect on initial anode air burning rate but as burn-off increases, the catalytic effect of vanadium plays an increasingly important role. It is probably significant that in published work (1) showing an excellent anode air burning vs. coke vanadium content correlation, air burning was carried out to a greater weight loss, 30%.

In contrast to the published work cited above, there was no statistical evidence for any effect of nickel or calcium on anode air burning rate, either

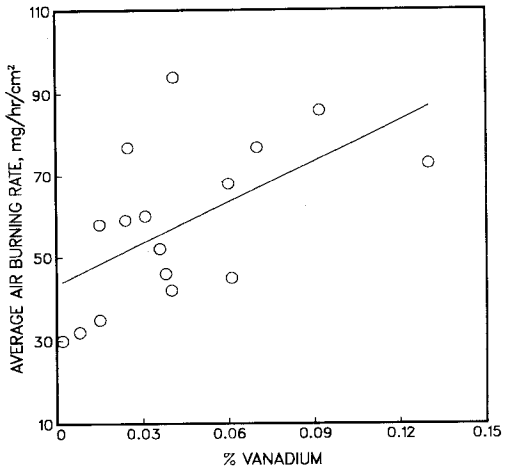

Figure 13. Average anode air burning rate to a 10% weight loss as a function of coke vanadium content.

overall rate to a 10% weight loss or rate during the last 30 mg of weight loss. (The R^2 values ranged from 0-15%.) It might be pointed out that the calcium correlation reported in the published work had a low R^2 value. The nickel correlation had an R^2 value of 62%, but the nickel and vanadium contents of the cokes tested were directly correlated to a considerable extent (23).

Excess Anode Consumption During Electrolysis

No single coke variable correlated very well with excess anode consumption. The best correlation was with coke nickel content (R^2=34%),* followed by silicon content (R^2=28%), and the sum of the metals content (R^2=26%). Ash content, which is related to the sum of the metals content, resulted in an R^2 value of 18%.

Although an effect of coke metallic impurities on excess anode consumption is not unreasonable and an ash correlation was reported previously (4), it was a concern that R^2 values as low as those given above might not be meaningful (despite the fact, as noted earlier, that a reference book considered an R^2 value as low as 25% to represent a moderate correlation). To test this concern, the excess consumption values were regressed against a number of sets of computer-generated random numbers instead of actual coke property data. In many cases, R^2 values for correlations with random numbers exceeded 34%. Hence, it can be concluded that some skepticism concerning the excess electrolytic consumption correlations is warranted.

Two-factor correlations resulted in R^2 values only up to 50%. Because correlation was still not very high, only the single variable equation for nickel content is given below:

*Coke No. 4 was a major outlier in these correlations. Since this coke had an atypical calcination history, and since the standard deviation for replicate consumption determinations was highest with this coke, elimination from the correlations was considered justifiable.

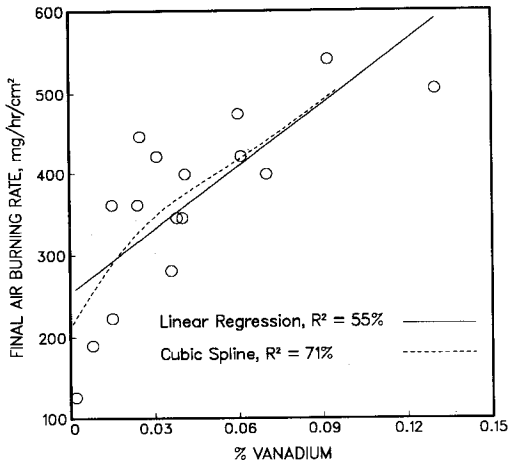

Figure 14. Anode air burning rate toward the end of a 10% weight loss as a function of coke vanadium content.

Consumption during electrolysis (in % of theoretical) = 106.0 + 39.7 x coke nickel content (in wt%).

Figure 15 shows consumption versus nickel content.

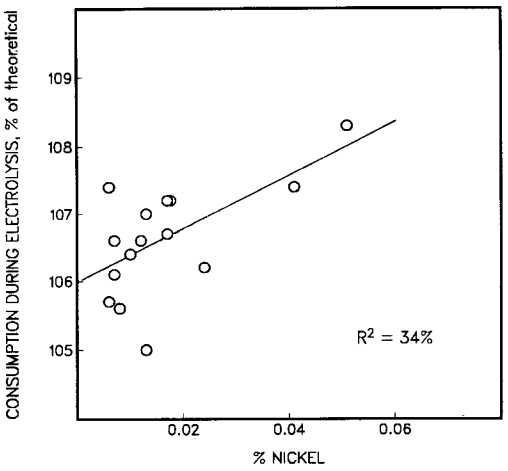

Figure 15. Anode consumption during electrolysis as a function of coke nickel content.

Excess electrolytic anode consumption is generally considered to be caused by preferential oxidation of binder coke, causing some filler coke particles to fall from the anode. Since nickel is a catalyst for many reactions, it seems likely that nickel would increase, rather than decrease, the calcined petroleum filler coke reactivity during electrolysis. Therefore, the increase in anode consumption with increasing coke nickel content could not be possible due to this mechanism. Possibly, one result of an increase in nickel would be to accelerate reaction in large coke pores, increasing the tendency of a portion of a petroleum coke particle to separate from the remainder of the particle.

RELATIONSHIPS AMONG ANODE PROPERTIES

There is little statistically significant evidence to suggest that a calcined coke that is desirable from the standpoint of one anode property is necessarily desirable with respect to other anode properties.

Only green and baked apparent densities correlated quite well (R^2=78%). Correlation of baked apparent density with average air burning rate was moderate (R^2=44%). Other correlations yielded R^2 values from 0-31%

SUMMARY

1. Correlations between each measured anode property and a maximum of two coke properties were derived by linear regression analyses, with R^2 values ranging from 34 to 96%.

2. The strongest correlation (R^2=96%) was for anode electrical resistivity as a function of -100+200 mesh coke resistivity, along with a coke vibrated bulk density measurement.

3. Very good correlations (R^2=87 and 90%) were found relating green and baked anode apparent densities to -28+48 mesh coke vibrated bulk density and terms indicating coke porosity below 5 μm in diameter.

4. Overall anode air burning rate to a 10% weight loss at 550°C correlated well only with pairs of porosity terms (maximum R^2=82%). Rate near the end of the air burning experiments correlated reasonably well with coke vanadium content (R^2=55% for a linear regression, 71% for a curvilinear regression).

5. Optimum anode binder level correlated reasonably well (R^2=66%) with -14+28 mesh coke vibrated bulk density, along with a measurement indicating coke porosity below 5 μm in diameter. Correlation may have been limited by the accuracy of the experimental optimum binder level determinations.

6. Correlations between anode consumption during electrolysis and coke properties were poor. The best correlation using a single coke property was with nickel content (R^2=34%). Reporting of a correlation with two coke properties is not considered to be justified.

7. Reasonable hypotheses in terms of chemical or physical interactions can be offered for all the correlations described above.

8. Except for a good correlation between green and baked anode apparent density (R^2=78%) and a moderate one between air burning and baked apparent density (R^2=44%), anode properties did not relate to other anode properties.

ACKNOWLEDGMENT

The authors gratefully acknowledge the assistance of Jeffrey W. Thomas, who carried out most of the experimental work on anode fabrication and testing. Special thanks is given to Kenneth C. Krupinski and Robert J. Osterholm of Aristech Chemical Corporation for supplying the anode air burning rate determinations.

REFERENCES

1. P. Rhedey: "Carbon Reactivity and Aluminum Reduction Cell Anodes," Light Metals 1982, The Metallurgical Society of AIME, Warrendale, PA, pp. 713-725 (1982).

2. G. J. Houston and H. A. Øye: "Reactivity Testing of Anode Carbon Materials," Light Metals 1985, The Metallurgical Society of AIME, Warrendale, PA, pp. 885-899 (1985).

3. W. Schmidt-Hatting, R. Perrushoud, and J. E. Durgnat: "Influence of Vanadium on Anode Performance," Light Metals 1986, The Metallurgical Society of AIME, Warrendale, PA, pp. 623-625 (1986).

4. P. J. Rhedey and S. K. Nadkarni: "Carbon Raw Material Effects on Aluminum Reduction Cell Anodes," Light Metals 1986, The Metallurgical Society of AIME, Warrendale, PA, pp. 569-574 (1986).

5. F. Keller and W. K. Fischer: "Development of Anode Quality Criteria by Statistical Evaluation of Operational Results in the Electrolysis," Light Metals 1982, The Metallurgical Society of AIME, Warrendale, PA, pp. 729-740 (1982).

6. P. Rhedey: "A Review of Factors Affecting Carbon Anode Consumption in the Electrolytic Production of Aluminum," Light Metals 1971, The Metallurgical Society of AIME, Warrendale, PA, pp. 385-407 (1971).

7. E. A. Kolodin and V. Ya Nikitin: "Effect of Coke Properties and its Calcination Conditions on Anode Consumption During Aluminum Electrolysis," Tsvet. Met., Vol. 8, pp. 44-45 (1982).

8. S. S. Jones, R. D. Hildebrandt, and M. C. Hedlund: "Influence of High-Sulfur Cokes on Anode Performance," Light Metals 1979, The Metallurgical Society of AIME, Warrendale, PA, pp. 553-574 (1979).

9. V. V. Burnakin, L. V. Arskaya, V. I. Zalivnoy, P. V. Polyakov, and V. F. Ofitserov: "The Use of High-Sulfur Cokes in the Production of Anode Paste," Tsvet. Met., Vol. 6, pp. 68-70 (1981).

10. E. Barrillon and J. Pinoir: "Use of High-Sulfur Cokes in the Production of Prebaked Anodes," Light Metals 1977, Vol. 1, pp. 289-299, The Metallurgical Society of AIME, Warrendale, PA (1977).

11. G. J. Houston and H. A. Øye: "Consumption of Anode Carbon During Aluminum Electrolysis (II)," Aluminium, Vol. 61, No. 4, pp. 346-349 (1985).

12. S. S. Jones and R. D. Hildebrandt: "Anode Carbon Reactivity," Light Metals 1974, Vol. 3, The Metallurgical Society of AIME, Warrendale, PA, pp. 901-932 (1974).

13. V. Ya Nikitin, L. N. Barashkova, and A. Ya Gorelik: "Effect of Heat Treatment of Cokes on Properties of Prebaked Anodes," Tsvet. Met., Vol. 6, pp. 56-57 (1983).

14. R. E. Gehlbach, E. E. Hardin, L. I. Grindstaff, and M. P. Whittaker: "Coke Density Determination and Its Relationship to Anode Quality," Paper presented at the 109th AIME Annual Meeting, Las Vegas, NV, Feb. 24-28 (1980).

15. D. N. Holdner and D. DuTremblay: "Production of Carbon Electrodes for Electrolytic Reduction Cells," UK Patent Application GB2116587A (Filed 16 March 1982; Application published 28 Sept. 1983).

16. R. T. Tonti, R. D. Hildebrandt, and M. F. Vogt: "Coke Isotropy and Its Effect on Anode Performance," Paper presented at the 113th AIME Annual Meeting, Los Angeles, CA, Feb. 26-Mar. 1 (1984).

17. V. D. Lazarev, E. A. Yanko, Yu M. Anokhin, I. P. Neudachina, and L. V. Lazareva: "Relationship Between the Properties of Coke and Anode Mix," Tsvet. Met., Vol. 1, pp. 49-52 (1982).

18. D. Belitskus: "Evaluating Calcined Coke for Aluminum Smelting by Bulk Density," Light Metals 1974, Vol. 3, The Metallurgical Society of AIME, Warrendale, PA, pp. 863-878 (1974).

19. R. F. Kohm and B. Novic, "Regression Analysis and Curve Fitting with ALSTAT," Alcoa Laboratories internal report, (Revised 1981 January 23).

20. M. S. Younger, "A Handbook for Linear Regression," Duxburg Press, North Scituate, MA (1979) p. 243.

21. Ibid.: p. 480.

22. P. Rhedey: "Structural Changes in Petroleum Coke During Calcination," Met. Trans, Vol. 239, pp. 1084-1091 (1967).

23. P. Rhedey (private communication, 1983 January 14).

Appendix 1. Coke Properties Determined and Range of Values

Property	Range	
1 = diameter under which 90% of -200 mesh particles occur, μm	67.4	132.3
2 = diameter under which 50% of -200 mesh particles occur, μm	25.4	50.2
3 = diameter under which 10% of -200 mesh particles occur, μm	4.8	21.0
4 = average particle size (volume basis) of -200 mesh, μm	31.7	74.1
5 = BET surface area, -4+8 mesh, m^2/g	0.13	0.82
6 = BET surface area, -28+48 mesh, m^2/g	0.17	1.40
7 = BET surface area, -100+200 mesh, m^2/g	0.41	2.90
8 = BET surface area, -200 mesh, m^2/g	1.0	5.2
9 = Ash, %	0.19	0.89
10 = Sulfur, %	0.96	4.45
11 = Aluminum, %	0.001	0.058
12 = Iron, %	0.004	0.069
13 = Silicon, %	0.003	0.100
14 = Nickel, %	0.006	0.084
15 = Vanadium, %	0.002	0.130
16 = Calcium, %	0.005	0.054
17 = Sodium, %	0.005	0.042
18 = Potassium, %	0.001	0.019
19 = Fluoride, %	0.000	0.045
20 = sum of Al,Fe,Si,Ni,V,Ca,Na,K,F; %	0.098	0.510
21 = resistivity of -28+48 mesh, μΩ•m	320	478
22 = resistivity of -100+200 mesh, μΩ•m	353	646
23 = resistivity of -200 mesh, μΩ•m	307	758
24 = sum of BET surface areas, m^2/g	1.80	10.01
25 = sum of total pore areas, 4 fractions, m^2/g	62.1	148.8
26 = sum of total intrusion volumes, 4 fractions, cm^3/g	1.70	2.13
27 = crystallite height as received, Å	27.9	42.3
28 = estimated coke calcination temperature, °C	1000	1350
29 = real density by helium displacement, g/cm^3	1.98	2.07
30 = real density by kerosine displacement, g/cm^3	1.98	2.09
31 = vibrated bulk density, -4+8 mesh, g/cm^3	0.634	0.910
32 = vibrated bulk density, -8+14 mesh, g/cm^3	0.746	0.911
33 = vibrated bulk density, -14+28 mesh, g/cm^3	0.756	0.993
34 = vibrated bulk density, -28+48 mesh, g/cm^3	0.853	0.972
35 = vibrated bulk density, -48+100 mesh, g/cm^3	0.846	0.993
36 = vibrated bulk density, -100+200 mesh, g/cm^3	0.882	1.059
37 = vibrated bulk density, -200 mesh, g/cm^3	0.869	1.119
38 = calculated aggregate VBD, g/cm^3	1.23	1.39
39 = aggregate VBD by method 424E, g/cm^3	1.132	1.308
40 = average vibrated bulk density, 7 fractions, g/cm^3	0.822	0.961
41 = weighted average vibrated bulk density, 7 fractions, g/cm^3	0.841	0.972
42 = average of -4+8 mesh,-28+48 mesh and -100+200 mesh VBD'S, g/cm^3	0.781	0.952
43 = average of -28+48 mesh, -48+100 mesh and -100+200 mesh VBD'S, g/cm^3	0.852	1.003
44 = average of -14+28 mesh, -28+48 mesh, -48+100 mesh and -100+200 mesh VBD'S, g/cm^3	0.828	0.983
45 = total pore area, -4+8 mesh, m^2/g	16.0	51.2
46 = total pore area, -28+48 mesh, m^2/g	14.1	41.6
47 = total pore area, -100+200 mesh, m^2/g	14.5	32.1
48 = total pore area, -200 mesh, m^2/g	13.6	24.9
49 = median pore diameter (volume basis), -4+8 mesh, μm	0.05	19.36
50 = median pore diameter (volume basis), -28+48 mesh, μm	36.0	99.7
51 = median pore diameter (volume basis), -100+200 mesh, μm	20.8	39.3
52 = median pore diameter (volume basis), -200 mesh, μm	3.6	15.6
53 = average pore diameter, -4+8 mesh, μm	0.013	0.070
54 = average pore diameter, -28+48 mesh, μm	0.029	0.084
55 = average pore diameter, -100+200 mesh, μm	0.112	0.206
56 = average pore diameter, -200 mesh, μm	0.095	0.217
57 = mercury porosimeter bulk density, -4+8 mesh, g/cm^3	1.304	1.591
58 = mercury porosimeter bulk density, -28+48 mesh, g/cm^3	1.116	1.438
59 = mercury porosimeter bulk density, -100+200 mesh, g/cm^3	0.772	0.896
60 = mercury porosimeter bulk density, -200 mesh, g/cm^3	0.768	0.894
61 = skeletal density, -4+8 mesh, g/cm^3	1.471	2.337
62 = skeletal density, -28+48 mesh, g/cm^3	1.974	2.478
63 = skeletal density, -100+200 mesh, g/cm^3	1.963	2.521
64 = skeletal density, -200 mesh, g/cm^3	1.451	2.170
65 = total intrusion volume, -4+8 mesh, cm^3/g	0.161	0.280
66 = total intrusion volume, -28+48 mesh, cm^3/g	0.210	0.401
67 = total intrusion volume, -100+200 mesh, cm^3/g	0.670	0.850
68 = total intrusion volume, -200 mesh, cm^3/g	0.487	0.776
69 = displacement density, 91 μm, -4+8 mesh, g/cm^3	1.383	1.622
70 = displacement density, 91 μm, -28+48 mesh, g/cm^3	1.302	1.587
71 = displacement density, 91 μm, -100+200 mesh, g/cm^3	0.759	0.876
72 = displacement density, 46 μm, -4+8 mesh, g/cm^3	1.437	1.668
73 = displacement density, 46 μm, -28+48 mesh, g/cm^3	1.342	1.688
74 = displacement density, 46 μm, -100+200 mesh, g/cm^3	0.839	0.917
75 = displacement density, 23 μm, -4+8 mesh, g/cm^3	1.497	1.729
76 = displacement density, 23 μm, -28+48 mesh, g/cm^3	1.364	1.739

Property	Range	
77 = displacement density, 23 µm, -100+200 mesh, g/cm^3	1.394	1.607
78 = displacement density, 9 µm, -4+8 mesh, g/cm^3	1.594	1.793
79 = displacement density, 9 µm, -28+48 mesh, g/cm^3	1.388	1.788
80 = displacement density, 9 µm, -100+200 mesh, g/cm^3	1.505	1.775
81 = displacement density, 5 µm, -4+8 mesh, g/cm^3	1.630	1.809
82 = displacement density, 5 µm, -28+48 mesh, g/cm^3	1.712	1.837
83 = displacement density, 5 µm, -100+200 mesh, g/cm^3	1.563	1.791
84 = displacement density, 1 µm, -4+8 mesh, g/cm^3	1.771	1.884
85 = displacement density, 1 µm, -28+48 mesh, g/cm^3	1.411	1.878
86 = displacement density, 1 µm, -100+200 mesh, g/cm^3	1.679	1.861
87 = -4+8 mesh, -28+48 mesh and -100+200 mesh average DD 91 µm, g/cm^3	1.223	1.313
88 = -4+8 mesh, -28+48 mesh and -100+200 mesh average DD 46 µm, g/cm^3	1.305	1.399
89 = -4+8 mesh, -28+48 mesh and -100+200 mesh average DD 23 µm, g/cm^3	1.467	1.655
90 = -4+8 mesh, -28+48 mesh and -100+200 mesh average DD 9 µm, g/cm^3	1.603	1.756
91 = -4+8 mesh, -28+48 mesh and -100+200 mesh average DD 5 µm, g/cm^3	1.633	1.789
92 = -4+8 mesh, -28+48 mesh and -100+200 mesh average DD 1 µm, g/cm^3	1.682	1.874
93 = displacement density, 5 µm, helium, -4+8 mesh, g/cm^3	1.625	1.811
94 = displacement density, 5 µm, helium, -28+48 mesh, g/cm^3	1.679	1.840
95 = displacement density, 5 µm, helium, -100+200 mesh, g/cm^3	1.557	1.784
96 = displacement density, 5 µm, helium, -200 mesh, g/cm^3	1.034	1.533
97 = -4+8 mesh, -28+48 mesh and -100+200 mesh average DD 5 µm, helium, g/cm^3	1.627	1.791
98 = displacement density, 5 µm, kerosine, -200 mesh, g/cm^3	1.039	1.601
99 = microporosity <5 µm, -4+8 mesh, cm^3/g	0.068	0.124
100 = microporosity <5 µm, -28+48 mesh, cm^3/g	0.060	0.112
101 = microporosity <5 µm, -100+200 mesh, cm^3/g	0.067	0.158
102 = microporosity <5 µm, -4+8 mesh, -28+48 mesh and -100+200 mesh average, cm^3/g	0.070	0.132
103 = median porosity, -4+8 mesh, cm^3/g	0.038	0.137
104 = median porosity, -28+48 mesh, cm^3/g	0.049	0.110
105 = median porosity, -100+200 mesh, cm^3/g	0.193	0.481
106 = median porosity, -4+8 mesh, -28+48 mesh and -100+200 mesh average, cm^3/g	0.106	0.164
107 = macroporosity, -4+8 mesh, cm^3/g	0.009	0.045
108 = macroporosity, -28+48 mesh, cm^3/g	0.070	0.207
109 = incremental volume at 91 µm, -4+8 mesh, cm^3/g	0.009	0.046
110 = incremental volume at 46 µm, -4+8 mesh, cm^3/g	0.006	0.018
111 = incremental volume at 23 µm, -4+8 mesh, cm^3/g	0.001	0.007
112 = incremental volume at 11 µm, -4+8 mesh, cm^3/g	0.001	0.010
113 = incremental volume at 91 µm, -28+48 mesh, cm^3/g	0.025	0.207
114 = incremental volume at 46 µm, -28+48 mesh, cm^3/g	0.008	0.017
115 = incremental volume at 23 µm, -28+48 mesh, cm^3/g	0.001	0.003
116 = incremental volume at 11 µm, -28+48 mesh, cm^3/g	0.001	0.004
117 = incremental volume at 91 µm, -100+200 mesh, cm^3/g	0.007	0.024
118 = incremental volume at 46 µm, -100+200 mesh, cm^3/g	0.012	0.173
119 = incremental volume at 23 µm, -100+200 mesh, cm^3/g	0.022	0.120
120 = incremental volume at 11 µm, -100+200 mesh, cm^3/g	0.008	0.021
121 = incremental volume at 23 µm, -200 mesh, cm^3/g	0.005	0.034
122 = incremental volume at 11 µm, -200 mesh, cm^3/g	0.010	0.176
123 = porosity >9 µm, excluding microporosity, -4+8 mesh, cm^3/g	0.045	0.174
124 = porosity >4 µm, excluding microporosity, -4+8 mesh, cm^3/g	0.053	0.130
125 = porosity >1 µm, excluding microporosity, -4+8 mesh, cm^3/g	0.070	0.228
126 = porosity >9 µm, excluding microporosity, -28+48 mesh, cm^3/g	0.073	0.304
127 = porosity >4 µm, excluding microporosity, -28+48 mesh, cm^3/g	0.147	0.311
128 = porosity >1 µm, excluding microporosity, -28+48 mesh, cm^3/g	0.085	0.341
129 = porosity >9 µm, excluding microporosity, -100+200 mesh, cm^3/g	0.487	0.754
130 = porosity >4 µm, excluding microporosity, -100+200 mesh, cm^3/g	0.512	0.764
131 = porosity >1 µm, excluding microporosity, -100+200 mesh, cm^3/g	0.556	0.792
132 = porosity >9 µm, excluding microporosity, -200 mesh, cm^3/g	0.121	0.576
133 = porosity >4 µm, excluding microporosity, -200 mesh, cm^3/g	0.212	0.633
134 = porosity >1 µm, excluding microporosity, -200 mesh, cm^3/g	0.406	0.712
135 = porosity <9 µm, excluding microporosity, -4+8 mesh, cm^3/g	0.073	0.137
136 = porosity <4 µm, excluding microporosity, -4+8 mesh, cm^3/g	0.068	0.124
137 = porosity <1 µm, excluding microporosity, -4+8 mesh, cm^3/g	0.052	0.107
138 = porosity <9 µm, excluding microporosity, -28+48 mesh, cm^3/g	0.068	0.236
139 = porosity <4 µm, excluding microporosity, -28+48 mesh, cm^3/g	0.063	0.233
140 = porosity <1 µm, excluding microporosity, -28+48 mesh, cm^3/g	0.046	0.224
141 = porosity <9 µm, excluding microporosity, -100+200 mesh, cm^3/g	0.077	0.183
142 = porosity <4 µm, excluding microporosity, -100+200 mesh, cm^3/g	0.069	0.158
143 = porosity <1 µm, excluding microporosity, -100+200 mesh, cm^3/g	0.050	0.114
144 = porosity <9 µm, excluding microporosity, -200 mesh, cm^3/g	0.195	0.550
145 = porosity <4 µm, excluding microporosity, -200 mesh, cm^3/g	0.138	0.481
146 = porosity <1 µm, excluding microporosity, -200 mesh, cm^3/g	0.064	0.174
147 = porosity >9 µm, excluding microporosity, 4 fraction average, cm^3/g	0.224	0.409
148 = porosity >4 µm, excluding microporosity, 4 fraction average, cm^3/g	0.261	0.429
149 = porosity >1 µm, excluding microporosity, 4 fraction average, cm^3/g	0.314	0.475
150 = porosity <9 µm, excluding microporosity, 4 fraction average, cm^3/g	0.119	0.222
151 = porosity <4 µm, excluding microporosity, 4 fraction average, cm^3/g	0.099	0.193
152 = porosity <1 µm, excluding microporosity, 4 fraction average, cm^3/g	0.055	0.123

APPENDIX II

DESCRIPTION OF THE MERCURY POROSIMETRY CALCULATIONS

Types of values given by the mercury porosimetry instrument:

total intrusion volume - the maximum volume of mercury penetration into the pores at the highest pressure.

total pore area - the area of the pore walls based on the assumption of cylindrical geometry and summed over the pressure range used.

median pore diameter (area) - the pore diameter at which equal quantities of pore wall area occur at larger and smaller diameters.

median pore diameter (volume) - the pore diameter at which equal quantities of pore volume occur at larger and smaller diameters.

average pore diameter (4V/A) - calculated from pore volume and pore area, based on the assumption that all pores are circular cylinders.

bulk density - calculated from the sample weight and volume at the initial mercury filling pressure.

apparent (skeletal) density - density of the sample as calculated for the bulk density and adjusted for pore volume measured at the maximum mercury pressure used (should be similar to real density for a -200 mesh fraction).

Additional types of values calculated using the information given by the instrument on total porosity in various pore size ranges:

incremental volume - the amount of mercury penetration into pores of a given diameter.

macroporosity - the volume of mercury penetration into pores with a diameter greater than 91 μm; calculated only for -4+8 and -28+48 mesh.

median porosity - the volume of mercury penetration into pores with a diameter greater than 5 μm but less than 91 μm; calculated for -4+8, -28+48, and -100+200 mesh.

microporosity < $\underline{n}$ - the volume of mercury penetration into pores with a diameter < $\underline{n}$ μm; calculated for all mesh sizes and for values of $\underline{n}$ equal to 1, 4, 5, and 9.

porosity > $\underline{n}$, excluding microporosity - the volume of mercury penetration into pores with a diameter > $\underline{n}$ μm; calculated for all mesh sizes and for values of $\underline{n}$ equal to 1, 4, 5, and 9.

average values - averages of the above values for combinations of three (-4+8, -28+48, and -100+200 mesh) and four (-4+8, -28+48, -100+200, and -200 mesh) coke fractions.

displacement density (DD$\underline{n}$) - a "pseudo" density derived by combining the inherent density of the coke (kerosine real density value) with the amount of microporosity less than a selected pore diameter $\underline{n}$ (in μm); calculated for -4+8, -28+48, and -100+200 mesh fractions for values of $\underline{n}$ equal to 1, 5, 9, 23, 46, and 91; for $\underline{n}$ = 5 displacement density was also calculated using real density values obtained from helium displacement; in addition, 5 μm displacement density was calculated for -200 mesh coke using real density values obtained from both kerosine and helium displacement methods; the formula for calculating displacement density is:

$$DDn = \frac{1}{P_{<\underline{n}} + \frac{1}{RD}}$$

where -

DD = displacement density
$\underline{n}$ = pore diameter in μm
P = microporosity in cm^3/g
RD = real density in g/cm^3.